An Evaluation of Linear Model Analysis Techniques for Processing Images of Micro-circulation Activity

John Mayhew*, Dewen Hu#, Ying Zheng#, Steve Askew*, Yuqian Hou*, Jason Berwick[⊥], Peter Coffey[⊥] and Nicky Brown[♣]

* Artificial Intelligence Vision Research Unit

#Department of Automatic Control and Systems Enginnering

University of Sheffield

[⊥]Department of Psychology, University of Sheffield

[♣] Hallamshire Hospital, University of Sheffield

Research Report No. 632

June 1996

An Evaluation of Linear Model Analysis Techniques for Processing Images of Micro-circulation Activity

John Mayhew, Dewen Hu, Ying Zheng, Steven Askew, Yuqian Hou, Jason Berwick, Peter Coffey and Nicky Brown

June, 1996

Abstract

Sequences of images of the cortical surface can be processed to reveal information about the cortical micro-circulation, regional cerebral blood flow (rCBF) and changes induced by neuronal activity. Images of rat sensory motor cortex and testes were processed using different analysis methodologies. The study examined the generalised linear model (GLM) approach, and compared the results with standard signal processing methods including principal component analysis (PCA). The GLM method has been used by Friston (1994) in the analysis of functional magnetic resonance imagery (fMRI) to identify regions of focal activity. We investigated the use of this method to analyse video image data of the modulation of rCBF from rat cortex. The results revealed spatio-temporal variations in rCBF in response to stimulation within local regions of cortex. The advantage of the GLM method is that it augments ordinary signal processing methods with an estimate of statistical reliability.

Using different wavelengths of illumination reveals different spatial structures with different temporal relationships. In image time series data collected under green and red illumination a phase difference was found in the low frequency ~0.1Hz vasomotion oscillation. This phase difference occurred in data from both cortex and testes. A possible explanation of these differences is that the spectral absorption characteristics of the tissue reflect changes in the volume proportions of the different hemoglobin derivatives in interacting with the modulation of the volume of blood known to occur. It is known that nitric oxide is involved in the modulation of the blood volume and flow, and that spectral changes occur as the nitric oxide is scavenged by hemoglobin to produce met-hemoglobin and nitrosyl-hemoglobin differentially produced in arterial and venous blood. It is proposed that the combination of these effects gives rise to the phase differences we detect.

1. Introduction

Recent developments in the use of video imagery have been used to investigate cortical functional architecture (Blasdel and Salama 1986; Grinvald, Lieke et al. 1986). These studies monitor the differential changes in image intensity produced under different stimulus conditions. Images under one stimulus condition, subtracted from images taken under another reveal functional structure. In *in vitro* preparations, similar imaging techniques have been used to investigate activity induced changes in the transmission characteristics of neural tissue (MacVicar and Hochman 1991; Andrew and MacVicar 1994). These studies are generally referred to as *intrinsic imaging* and a review, evaluation and simulation study of the intrinsic imaging methodology can be found in Mayhew and Zheng (1996). Video imaging is also increasingly used to investigate the micro-circulation and the regulation of rCBF by neural activity (Woolsey and Rovainen 1991; Cox, Woolsey et al. 1993). In the latter case the major variables are changes in the dimensions of the surface microvasculature, transit times and velocities. These are measured using standard image processing techniques. Recently we have begun to exploit intrinsic imaging in the investigation of the neural activity induced changes in the micro circulation and in particular the investigation of the low frequency oscillations in rCBF (Mayhew, Askew et al. 1995; Mayhew, Askew et al. 1996). We refer to these low frequency oscillations as the V-signal to distinguish them from the increases in blood flow and volume which are generally referred to by the term rCBF.

Our data consists of a sequence of 2D images of the reflectance of the surface of the brain taken under different conditions of stimulation. The sequences often last several minutes and are captured at video frame rates. As a data sequence this may be regarded as a 2D analogue of the 3D data sequences characteristically captured in fMRI though with much finer spatial and temporal resolution. The grey level variation over time of each pixel in the image provides a time series. These can be processed using standard linear and non-linear signal processing techniques. In this study we explore the use of linear and multivariate statistical techniques previously evaluated by Friston and colleagues in the analysis of fMRI data sequences. Some of the details of these methods can be found in standard texts but we know of no easy guide to the others, so to aid the reader brief descriptions are included in Appendix I.

2. Materials and Methods

2.1 Imaging

Images were captured using a Panasonic camera (WV-BL602) and a Leica operating microscope (MZ 6). The images were digitised to 8 bits and a 200 x 200 pixel region of interest was stored direct to disc using an SGI Onyx computer equipped with a Sirius Video board. At the magnification used this corresponds to a 2 by 2 mm region of cortex (1 pixel = 10 microns). Illumination, matched for intensity at wavelengths 565nm and 660nm was by LEDs (L-53S) (FWHM <30nm) Home brew electronics were used to drive the LEDs and the video signal was used to trigger them so that alternative fields were illuminated with different wavelengths (the illumination cross talk between successive fields was less than 3%). This allowed the near synchronous collection of images under different illumination at the cost of reducing the vertical resolution by half.. The aspect ratio was restored by spatially smoothing the images with a 2:1 elliptical mask and subsampling appropriately to give a final pixel resolution of 20 microns.

2.2 Subjects

Anaesthetised (urethane 1.3mg/kg) male Sprague-Dawley rats (280-320g) bred in the Sheffield Psychology Department laboratory were used. After anaesthesia induction the femoral arteries were cannulated for the purposes of monitoring MABP and for exsanguination. The animals were then placed in a stereotaxic frame and the dorsal surface of the skull thinned to provide a closed *cranial window* through which the surface of the brain could be viewed. A shallow well (sculpted from dental cement) surrounding the window and filled with saline minimised specular reflections. The systemic parameters: heartbeat, breathing and blood pressure, were monitored and the rectal temperature was maintained at 37°C using a thermostatically controlled heating blanket. The femoral arteries were cannulated for the purposes of monitoring MABP and for exsanguination.

2.3 Experimental Procedures

Representative data from three experiments were selected for the evaluation of the different methods of analysis. The physiological relevance of the experiments will be reported elsewhere, the emphasis in this report is on the methodology of the analysis. The experimental data are from the following experiments:

Experiment 1: The effects on rCBF in sensory cortex produced by a tail pinch of moderate intensity. Data was collected for total of 41 seconds (1025 video frames). Starting on frame 513, a tail pinch was administered lasting two seconds (50 frames).

Experiment 2. The effects on rCBF in sensory cortex produced by exsanguination were examined. Baseline data was collected for 30 seconds before MABP was reduced by slowly withdrawing 1 ml of blood over a period of several seconds. Blood pressure was allowed to stabilise and then a 2nd ml of blood was withdrawn over a period of several seconds followed by another period of stabilisation before a 3rd and final ml was withdrawn. The modulation of rCBF was monitored continuously using video data.

Experiment 3. The modulation of local blood flow in rat testes. There was no intervention other than the exposure of the testes as part of a cremaster muscle preparation. Video data was collected over a period of 3 minutes.

3. Results and Discussion

The strategy we adopt is to first perform an analysis of the experiments using well tried signal processing techniques. This preliminary stage of processing is used to inform and direct the subsequent stages of the statistical analysis. We then evaluate the correspondence between the different approaches, with particular emphasis on whether one can determine a measure of the statistical confidence in the conclusions.

3.1 Preliminary Analysis of Experiment 1

At isobestic wavelengths reflectance changes due to hemoglobin absorption are independent of the state of oxygenation of hemoglobin and thus changes under the 565nm illumination are predominantly due to volume changes. At 660nm changes in absorption may be due to either changes in volume or changes in state of oxygenation. Under 565nm illumination both arterioles and venules are apparent in the surface microvasculature, whereas under 660nm illumination the venules are more visible than the arterioles.

Figure 1(a, b) shows pseudo colour plots of the mean images from the first 512 frames of Experiment 1 under the green (565nm) and red (660nm) illumination conditions. There is a clear difference in the visible microvasculature in the two images which is used to classify the image outlined regions as venules(1), arteriole(2) and parenchyma(3). Figure 1(c,d) shows the time series of the mean over the image for the different illumination conditions. We use the term *mean image* to refer to the image produced by collapsing the data sequence over time. We use the term *mean time series* to refer to the time series produced by taking the average grey level of each image or region of interest. From Figures 1c and 1d we can see: i) that the response under the two illumination conditions are very different, and ii) that there is evidence of a low frequency oscillation in both time series.

Analysing the data at higher spatial resolution, Figure 2(a,b,c) shows smoothed mean time series under the different illumination conditions from regions designated as venules, arterioles and parenchyma in Figure 1. It can be seen that in veins and parenchyma there are clear differences in the response to the stimulation under the different illumination conditions. In contrast, in the region classified as arterioles the time series under the two illumination conditions are somewhat similar and show clear evidence of the presence of the V-signal oscillation. In these regions there is little evidence that the response to the stimulation was an increase in volume *per se*. This would have increased absorbance and produced a decrease in the time series amplitude following the stimulus.

Figure 3 shows the results of principal component analysis (PCA) applied to the image sequences under the different illumination conditions (details of the procedure are given in Appendix II). Figure 3(a,b) shows the first twenty eigen values, only the first 4 to 6 are of significant. Figure 3(c,e) shows the eigen vectors corresponding to the first four highest eigen values. Figure 3(d,f) shows a mosaic of the corresponding 'eigen images'. One should note the difference between the structures revealed under the different illumination conditions. It is difficult to interpret the higher order eigen images (Friston has recommended the use of canonical variate analysis in this situation), however the first PCA clearly reveals activity in very different areas in the two illumination conditions.

Figure 4(a,b) shows correlation maps produced by taking the correlation (pixel by pixel) of the time series under the two illumination conditions with the time series of the hemodynamic models. They show maps of the *'lags of the maximum correlation'* and the values of the correlation at those lags. Figure 4(a1, b1 and a3, b3) are produced by correlating the time series of the hemodynamic model P1 and P3 (see below) with the sequence under red illumination, and Figure 4(a2,b2) show the map produced by correlating the time series obtained under green illumination with the hemodynamic model P2 (see below) These correlation maps reveal spatial structure by showing areas which have similar temporal relationships, and as can be seen, there is considerable spatial structure in the mosaics under both conditions of illumination. This implies that response to the stimulation occurred with different lags at different spatial positions. These lags will be used in the subsequent application of the GLM method described below, but in the interim, it is important to note that the clear disassociation of the P1 and P2 models and that the red and green undershoot occur at different times in the two data sequences.

The physiological significance of this data is discussed below. However we will briefly make the following points:

- The area of cortex is of the same size which is typically monitored using laser Doppler flowmetery which produces a single time series. Mayhew et al (1995) have shown the

similarity between the mean time series from optical imagery and concurrent laser Doppler flowmetery (LDF).

- When analysed on a regional basis it can be seen that even at this resolution, the data contains considerable spatio-temporal variation which is different under the two illumination conditions. The time series under red and green illumination reveal different spatial structures with different time courses.
- The data contains an oscillatory component which is present before the presentation of the stimulus upon which is superimposed the response to the stimulation. We refer to this low frequency oscillation as the V-signal and believe it to be the imaging analogue of the vasomotion signal measured using LDF.

The purpose of the study is to evaluate the GLM methodology for analysis of intrinsic image data and whether it is possible to establish the statistical reliability of the above descriptive analyses using this technique.

3.2 The use of GLM to monitor changes in rCBF.

3.2.1 The Generalised Linear Model.

This method was proposed by Friston and colleagues (Friston, Frith et al. 1991; Friston, Jezzard et al. 1994; Friston, Worsley K et al. 1994) in the context of the analyis of fMRI data. In its simplest form the method uses least squares to solve a linear equation of the form $X = G \cdot \beta + e$ using the pseudo-inverse. X is the data vector, G the design matrix, β a vector of coefficients and e is random noise. Least squares estimate of b is given by the expression

$$\beta = (G^T \cdot G)^{-1} \cdot G \cdot X^T$$

The situation differs slightly when the data has been smoothed and subsampled. The primary effect of smoothing the data is to colour the noise. Least squares assumes that the noise is white. However, because the data is very noisy and the signal to noise ratio low we smooth and subsample the data both spatially and temporally. Thus the original expression above becomes

$$K \cdot X = K \cdot G \cdot \beta + K \cdot e$$

where K is the appropriate convolution matrix. The effects of this are: i) to modify the analysis (see appendix for the mathematical details) to take into account the correlation which colours the noise, and ii) to change the number of the effective degrees of freedom and hence the estimation of the residual. The details do not concern us now. However it is important to realise that the GLM method is applied to the individual pixels completely independently. For each pixel the result is a vector of parameter values and an associated residual matrix containing the errors. These can be used to scale the parameter values to provide a statistic satisfying a t-distribution. We refer to the statistic as the 'z' score, and the images produced by plotting the 'z' score of each pixel as a grey level, as statistical parameter maps (SPMs).

3.2.2 Tests for Significance.

An issue that is not totally resolved is how to choose the threshold of the 'z' score appropriate for a particular level of statistical significance. Appendix I contains technical details from Worsely (1992) and Friston et al (1994). Briefly the method selects a threshold value that is scaled by the confidence level, the number of pixels in the image and the spatial scale of any

smoothing function used. The resulting threshold is somewhat conservative. Intuitively, *so many 'tests' are being done that some false positives will occur by chance (distributed in small patches over the image) so a stiffer criterion must be used.* An alternative method is to chose a lower threshold. Thresholding at this level produces regions of connected pixels of different sizes. It is then possible at this level of 'z' score to select a confidence level. The method (Friston, Worsley K et al. 1994) then provides a *size* threshold. The size of the regions of connected pixels with 'z' scores above that level can be used to assign a level of significance to that particular region Regions equal or greater in area are considered statistically significant. Intuitively, *so many tests are being done that some false positives will occur by chance (distributed in small patches over the image) but if these 'false positives' occur in connected regions greater than a certain size we can consider them significant.* This is effectively the same as choosing a 'z' score threshold appropriate to the size of the region (number of pixels) that one regards as being in some sense 'significant' based on expectations from prior information. The formulae for these operations are given in Appendix I.

In what follows we have chosen to present the SPMs unthresholded in most cases but where appropriate overlaid with the 95% confidence 'contour' given by the conservative method of estimating the statistical significance. This is only in part because we had no principled prior expectations of spatial scale with which to select the area of pixels to use as the size threshold.

3.2.3 Designing the Design Matrix

The structure of the design matrix is the important feature of the method. It has as many rows as there are data, i.e., its columns are explicit time series which reflect the statistical model of the experiment. Thus some columns contain temporal models of the neuro-hemodynamic responses, others contain components of the V-signal, ramps to capture linear trends in the data etc., while others simply reflect the order of the experimental conditions. Thus the number of columns is the same as the number of parameters that are to be estimated using least squares. Associated with every pixel there is a data vector (a time series of the raw grey level intensity of the pixel), and a design matrix of the same length and as many columns as there are parameters. To illustrate: in the cortex of Experiment 1, the design matrix contains a parameter corresponding to a DC or constant time series, but because there was no obvious trend, a ramp was not included. To extract the 0.1 Hz V-signal, a unit sine and cosine time series with a frequency of ~0.1Hz are used to estimate the amplitude and phase. The actual frequency used was estimated from a preliminary analysis using *non-linear least-squares* (Levenberg-Marquardt) analysis applied to the first 512 (before stimulation) frames of the mean time series. Interestingly we find a 10% difference in the frequencies under the two illumination conditions (0.1133 and 0.1011 Hz under 565 and 660 nm respectively).

Three other vectors are used in the design matrix. They are time series representing neuro-hemodynamical responses. These are modelled using differently parameterised gamma functions. The parameters of the neuro-hemodynamics functions were estimated from the mean time series for the different illumination conditions using *non-linear least squares*. Because the structure to be used in the final analysis is a linear sum, the non-linearity in this stage of the analysis is confined to the estimation of the parameters of functions combined in a simple additive way. We refer to the parameters of neuro-hemodynamic functions as P1, P2, and P3. They are characterised by different delays and widths (corresponding to the mean and variance of the gamma functions used as models). P1 and P3 represent the undershoot and subsequent overshoot under red illumination. P2 represents the post stimulus response under

green illumination. These time series are the models of the hemodynamics used in generating the correlation maps described above.

The estimation of the V-signal parameters is done using the same additive model. The *designing* of the design matrix is a complicated art form needing both good taste, perseverance, and several passes through the data. One particular problem in this application is that the V-signal is not always easily represented as a simple sinusoidal oscillation. We are currently exploring the use of an adaptive tracking strategy to provide a parameterised model of the V-signal oscillation.

After the design stage the data time series for every pixel is smoothed and subsampled. Exactly the same smoothing procedure is then applied to every column in the design matrix using the convolution matrix *K*. We used two different smoothing and sampling strategies. One used a running window with a forgetting factor of 0.9, and subsampled the data and design matrix every 10 frames. The other simply averaged successive blocks of 10 frames. The primary difference is that the second method has no effect on the colour of the noise which remains white. The manipulation had no important effect on the results and thus the experiments we report here all used the running window smoothing method.

Figure 5 shows the three hemodynamic models used in the design matrices for the first study. The design matrix also contained vectors for DC, and sine and cosine terms to model the V-signal. In this first study there was no compensation for the different temporal lags revealed in the correlation maps, but they were used in subsequent analyses.

3.2.4 The Analysis of the Data

Figure 6 shows parameter maps (PMs) for the two illumination conditions in which the value of the parameters is represented in pseudo colour and scaled to make use of the whole range. These maps are not statistical parameter maps (SPMs). They represent only the value of the parameters, not estimates of their statistical reliability. Figure 6(a) shows PMs corresponding to the amplitude of the hemodynamic response functions. Figure 6b shows the spatial distribution of the amplitude of the V-signal. It is obtained by taking the square root of the *sum of the squares* of the parameters for the sine and cosine functions. Figure 6c shows the corresponding phase map. It is the arctangent of the ratio of the parameters for the sine and cosine functions.

Figure 7(a,b,c) show the corresponding SPM(z) for the above maps, P1, P2 and P3. These show the distribution of the 'z' scores. The SPM(z)s for the amplitude of the V-signal are not shown as they convey little more information than the parameter maps and reached statistical significance only in few small regions.

Subject to the appropriate reservations concerning their statistical significance, the PMs of V-signal parameters are not spatially homogeneous (Figure 6b,c). We find that both the phase and amplitude maps differ under the two different illumination conditions. The amplitude (Figure 6b) picks out different regions not confined to the different types of surface vascularity. The phase of the V-signal (Figure 6c) also shows spatial variation across the image. These results suggest that the V-signal is not confined to the surface microvasculature but is present in the underlying capillary beds in parenchyma. We will show further evidence from other experimental data that supports these conclusions.

The parameter maps of the hemodynamic response models under both illumination conditions reveal varied spatial structure. There is considerable and obvious correspondence with the surface microvasculature, however much of the significant activity occurs in regions where

there is little surface microvasculature and in these regions the signals are derived from the underlying capillary beds.

- *P1 (delay: peaking at ~4 seconds)* This parameter models the mean time series decrease in intensity preceding the overshoot under red illumination. An interpretation of the SPM(z) under red illumination is that it shows areas corresponding to a significant decrease in intensity derived primarily from a reduction in the proportion of oxygenated hemoglobin and related changes in the absorption spectra of hemoglobin induced by increased neural activity, rather than from an increase in blood volume *pe se*. Of particular note is region 1. This area, in a vein, does not show a significant change. At a coarse scale the map shows the maximum activity occurring in the right bottom image quadrant.

- *P2 (delay: peaking at ~7 seconds)* This parameter models the mean time series decrease in intensity seen under green illumination. The SMP(z) shows a statistically significant response overlapping almost all the imaged area as shown by the P1 map, but with increased vascular detail which shows up as areas which don't reach significance. PCA (Figure 3) under green illumination also has greater vascular detail than under red. The 'peak' of the activity appears in region 2 which we believe to be an arteriole. There is a region clearly corresponding to a major blood vessel (region 1) which shows no significant change under the green illumination. It seems that the P2 parameter is relatively *blind* to the activity of veins and venules.

- *P3 (delay: peaking at ~13 seconds)* This parameter models the mean time series overshoot or rebound in image intensity under red. The SPM(z) shows significance over all the imaged region. The obvious spatial structure shows very high activity in the previously insignificant areas revealed in the P2 map.

The interpretation of the maps is not quite straight forward. The intensity of a pixel at any point in the image is potentially produced by a combination of at least three sources. These are from veins and venules, arteries and arterioles, and from the underlying parenchyma. The measured time series at any point is thus a spatio-temporal function of signals which will depend on the order of the sources down the line of sight (a pixel from a region of vein overlying an artery which itself is lying on the parenchyma will have a different time series from one in which the artery overlies the vein). Evidence of this mixing of sources can be seen at several places in the above maps.

Given this general caveat, we conclude from this analysis that the effect of stimulation was to produce a transient decrease in the blood oxygenation (either by reduction to Hb or to metHb) later followed by an increase in blood volume and flow. The evidence for the increase in flow is the large overshoot in intensity suggestive of hyper-oxygenation of both the venules and parenchyma. This conclusion is in contrast to that reported by Turner and Grinvald(1994) in monkey cortex. They suggested that capillaries in active tissue do not become hyper-oxygenated and that only draining venules do so. However we find the overshoot commonplace in our studies, occurring regularly in both venules and parenchyma. The discrepancy may have arisen because of the differences in the illumination wavelengths used. We cannot comment on Turner and Grinvald's conclusion that BOLD MRI techniques will be likely to fail to localise cortical structures of the scale of the ocular dominance columns but the above analysis (of a single trial) suggests the deoxygenation and subsequent hyperoxygenation response to a tail pinch in rat occur over an area about a 2 mm square.

In order to examine the stability of the maps we obtained above, we repeated the study while modifying the design matrix in several ways to answer the following questions.

(a) What is the effect of including inappropriate models in the design matrix?

We repeated the above study using all three models in the design matrices for the different illumination conditions, (e.g., the analysis under green illumination included hemodynamic models P1 and P3 as well as P2). We do not show the results but the maps obtained were very similar to those shown above.

(b) The accuracy of the models and correct temporal positioning.

If the models used in the design matrix are incorrect then although least squares will do its best, it might not be good enough. We have found that the particular shape of the bump functions used to model the hemodynamics is not particularly important in determining the spatial structure of the resulting maps. For example the use of appropriately positioned and scaled Gaussians gave near identical results to those obtained using gamma functions as did the use of the mean time series as the model. If the data has little noise, the model is a parameterised function, and if the computational expense can be met, one could simply use non-linear least squares to fit the model parameters for each pixel time series independently and compare the distribution of the parameters under different experimental conditions.

To evaluate the sensitivity of the method to the temporal positioning of the hemodynamic model functions the time series for each pixel was correlated with the general model (e.g., the one obtained from the mean time series) to find the 'appropriate' lag. The model was then shifted accordingly for each pixel. As this involves forming individual design matrices for every pixel, it makes the algorithm slightly more complicated and obviously incurs computational overhead. The benefit is that the map of the lags reveals the temporal structure of the different responses and the parameter maps show the amplitude of the responses unconfounded with any differences in their timing. Figure 8(a,b,c) shows the corresponding SPM(z)s. Though almost indistinguishable from those shown in Figure 7 the maps in Figure 8 are in a sense more correct given that we know from the correlation maps that the data is temporally heterogeneous.

There are other strategies for dealing with the temporal differences. For example, each of models P1, P2, P3 could be independently modelled as the sum of temporal basis functions, and GLM straightforwardly applied to find the blend of the parameters that optimally fits the data. This is formally what happens using sine and cosine functions to model the V-signal. The choice of strategy depends on the identification of theoretically relevant constraints on both the model and the interpretation of the results.

(c) What is the effect of excluding the V-signal from the design matrix?

We examined this question for several reasons. Firstly some people simply ignore the presence of the V-signal relying on averaging techniques to remove it. Secondly, it cannot easily be removed from the data by bandpass filtering because of the overlap with the neuro-hemodynamic responses. In the previous analysis of the data the parameters for the V-signal amplitude did not reach significance and not surprisingly excluding the V-signal from the design matrix has little effect on the spatial maps for the hemodynamic parameters.

However, the map of the residual shows clear evidence of structure, and the Fourier spectrum shows clear peaks in the low frequency region. Figure 9(a,b) shows three comparison maps of the variance of the residual from different analyses under the (a) green illumination and (b) red illumination. The design matrix included : i) the appropriate hemodynamic models without correction for lags and without the V-signal components (the left maps); ii) components to extract the V-signal but no correction for lags of the hemodynamic parameters (the centre

maps); and iii) components to extract the V-signal and lags of the hemodynamic. We find the lag correction has almost no effect whatever on the residual maps and that the very obvious structure in the residual maps is largely produced by very low frequency signal of ~0.05 Hz.

This obvious spatial structure in the residual maps is clear evidence that more sophisticated methods of analysis is needed. One possibility is to first use the hemodynamic models and GLM to remove activity induced changes from the data, then the residual time series can be further analysed using multi-taper methods of spectral analysis (Thomson 1982; Thomson and Chave 1991) to reveal the spatio-temporal structure of the V-signal. We are currently exploring both these methods.

(d) The use of the mean time series in the design matrix.

If this is ever appropriate, it is so only when there is no temporal variation across the image (e.g., if the correlation mosaic shows no spatial structure), and there is no other way of obtaining a model. It is quick, dirty and biased but worth a look.

3.3 The use of GLM to investigate the V-signal

In this and in the following section we use GLM to investigate the spatial structure of the V-signal using data from two preparations unconfounded by changes in rCBF in response to sensory stimulation. In the first, we analyse data from an experiment monitoring the effect of reducing the MABP by exsanguination (a replication of an experiment by Morita et al (1992)), and in the second, the V-signal from rat testes was explored without any physiological intervention.

3.3.1 V-signal in cerebral cortex

Modulation of rCBF by reduction of MABP.

Exsanguination produced a rather obvious change in the amplitude and frequency of the V-signal. Figure 10(a) shows the time series of the MABP and Figure 10(b) shows the mean time series of the data collected under red and green illumination. It can be seen that there is a degree of correspondence between the green and red time series until after the second blood withdrawal. We do not have a complete explanation for this decoupling of the two signals, though we have found it in other experiments in this preparation, and is currently a phenomenon awaiting further exploration.

The GLM analysis was used to reveal maps of V-signal amplitude and phase and to compare the differences before and after the first withdrawal of blood. Non-linear least squares was used to identify the frequency under each illumination condition and for each section of the data. Before blood withdrawal they were 0.094 and 0.095 Hz for the green and red conditions respectively, and after withdrawal they were 0.0791 and 0.0788 Hz. A similar change in frequency after withdrawal has been described by Morita et al (1992). The design matrix was partitioned into *before* and *after* exsanguination sections. It included sine and cosine functions of the appropriate frequencies (0.094, 0.079) and DC and linear trend terms for the amplitude of the sine and cosine functions. The maps of the amplitude are shown in Figure 11(a) and the phase maps are shown as arrows superimposed on images of the surface vascularity in Figure 11(b) for the two illumination conditions. The maps reveal spatial inhomogeneties in the amplitude of the V-signal which is not confined to the surface vascularity and is different under the two illumination conditions. Under green illumination, although the V-signal was present everywhere, 'peak activity' was confined to a relatively small region. The maps

showing the phase of the V-signal are different under the red and green illumination and histograms, weighted by amplitude, support this and show that the V-signal under red illumination leads by ~0.5 radians which at this frequency is slightly less than a second. It is noticeable that the phase structure of the maps is more coherent after blood withdrawal. In the case of the phase map under green illumination before withdrawal, the 'jitter' in the angle map may have been produced by the rather small amplitude of the V-signal.

The problem then is how to test for the significance of the difference between the amplitude of the V-signal before and after withdrawal. This would be straight forward if it were simply the comparison of a single parameter, but the amplitude is given by the square root of the sum of the squared coefficients for the sine and cosine parameters. One strategy is to use the first pass of the data to estimate (for each pixel) the phase of the sinusoidal oscillation. This is then put into the design matrix as a single explicit model. The analysis is then repeated but with a single parameter for the V-signal oscillation. Direct comparison is now possible between the conditions using the contrast vector (this is used to apportion the variances appropriately; see Appendix I).

Figure 11(c) shows the SPM(z)s of the difference between the conditions using this strategy. A histogram of the amplitudes of the V-signal before and after the withdrawal of blood showed clear differences under both illumination conditions. However, the SPM(z) maps of the pre and post withdrawal difference under both green and red illumination show spatial structure but neither reached significance. This is despite the fact that under red illumination there was an increase in amplitude in the time series of every pixel. Histograms of the 'z' scores of the *before, after and difference* maps under the different illumination conditions suggest that our naive use of Worsley's method (Worsley, Evans et al. 1992) for calculating the significance level is too conservative. However, in this data, it is not clear what more information would be gained over and above that already displayed in the SPMs by arbitrarily lowering the threshold and adopting the region counting strategy (described above and in Appendix I). This produces several large regions with extremely high confidence levels but of not much *significance*. Not withstanding, the results of the analysis are interesting. The changes in signal produced by exsanguination have no reliable correspondence with the surface microvasculature, and of particular importance (and completely unpredicted) was the finding of the phase difference under the two illumination conditions. This will be discussed after the analysis of Experiment 3 below (re-examination of the V-signal data from Experiment 1 also revealed a phase difference under the two illumination conditions, though smaller than in Experiments 2, and 3).

3.3.2 V-signal in periphery

Modulation of blood flow in rat testes.

This analysis used GLM to evaluate data from an experiment examining the spatial distribution of phase and amplitude of the V-signal in peripheral tissue (rat testes). The importance of this data for the present study is that it presents an interesting analysis problem, however the data has important physiological implications. We find an obvious and significant phase difference between the mean time series of the V-signals under red and green illumination. This awaits a full explanation, however, it is clear that this phase difference is a challenge to the idea that the V-signal is a simple modulation of hematocrit. Figure 12a shows the mean image under the green illumination with the location of the surface microvasculature (little of which is visible under the red illumination which implies that it is predominantly arterial). From the mean time series under red and green illumination conditions (Figure 12b) it is clear that not only is there

a large phase difference between the red and green signals, but that the amplitude of the V-signal changes over time, and that under the green illumination it is considerably larger than under red. This data requires a slight increase in complexity in the design matrix. The parameters for the amplitude of the sine and cosine terms are linear trends (the design matrix also included DC and linear trend terms). Non-linear least squares estimates of the frequencies of the V-signal were 0.0938 and 0.0926 Hz for the green and red illumination conditions. We used 0.0938 Hz in the design matrix for both. Figure 13 shows the results of the analysis. Figure 13 (a, b) show amplitude and phase maps. Angle maps in which the phase of the V-signal is represented as arrows superimposed on images of the surface vascularity are shown in Figure 13(c). The analysis reveals differences between the two illumination conditions in the major vessel on the right of the image. Under green illumination the amplitude of the V-signal in this area is very small and not significant (in contrast to the amplitude in the same area under the red illumination condition). Thus in this region the phase angle maps under green should be considered unreliable. However the differences revealed by the illumination conditions are not confined to the obvious surface vasculature but are also present in areas where the signal are derived from the underlying capillary beds. The V-signal under red illumination leads the V-signal under green, histograms of the phase maps showed no overlap and the peaks of the distribution are separated by more than a radian which at this frequency corresponds to ~1.7 seconds. It is possible using GLM that errors in the estimated frequency used in the design matrix can show up as phase differences. This is unlikely in the above analysis as the differences are so large, nevertheless an alternative method for analysis of simple oscillatory signals, complex demodulation (CDM, see Appendix III) was used to test for the variation in frequency. Figure 14 shows maps of the frequency estimated using iterated CDM under the two illumination conditions. Under green illumination there is little variation in frequency where as under red the results suggest a drift from bottom right to top left. The same direction of trend can be seen in the phase map shown in Figure 13(b).

4. Summary

4.1 Analysis methodology

We have described here the use of GLM (general linear models) in the analysis of experiments exploring activity in both cerebral and peripheral micro-circulation. The spatial structure revealed in the statistical parameter maps was tested for statistical reliability using the methods described by Worsely(1992) and Friston (1994).We find that GLM can usefully augment the basic repertoire of classical signal processing methods particularly in analysing data in which changes in rCBF arise in response to neural activity. In this case, models of the neuro-hemodynamics can be exploited. These models can either be obtained from the data as described above or from other sources. On the other hand we have reservations about its use as a tool for the examination of the V-signal due to its spectral complexity.

The methods for thresholding the SPM(z)s are independent of whether or not GLM is used in the analysis, however, we believe there are still developments needed here. They may not wholly applicable to the sort of data we have, though they are sufficiently conservative that we have no reservations about the conclusions we have drawn. They were designed primarily to distinguish regions of increased activity in the context of the null hypothesis that a smoothed Gaussian random field would present regions of high activity with certain height and scale purely by chance. Developed in the context of detecting regions of focal activity in PET and fMRI data, it is really only appropriate in analyses to detect relatively small bounded regions of

activity, and not in our case when the maps show large complex structures containing holes and bounded by image edges that in a strict sense violate the mathematical assumptions underpinning the method. We are currently investigating this issue in greater detail.

We believe that a better approach to the examination of the structure of the V-signal is to use multi-taper-window spectral analysis spectral analysis and jackknifed error estimates (Thomson 1982; Thomson 1990; Thomson 1995). This methodology has recently been exploited by Mitra et al (1996: personal communication) to examine the spatial structure of ~0.1Hz oscillations in fMRI data sequences. One possibility is to exploit these advanced multi-taper window methods on the residuals following a preliminary pass through the data using GLM to remove the neuro-hemodymic responses and trends. In the context of the investigation of the spatio-temporal structure of the V-signal we believe the most appropriate strategy to be the use of spectral coherence analysis (this is currently being explored and will be the subject of a subsequent report).

The use of this method will not finesse the issue of how to choose the significant level for spatially distributed SPMs, but there is an important shift in emphasis. If the question being asked is *what are the values of the parameters and how reliable are their estimates* rather than *are the measurements greater in this area than in that one* then different methods may be more suitable in one case than in the other. It is certain that more than one method of analysis will be needed and the importance of the developments by Worsely(1992) and Friston (1994) will increase in analyses where known anatomical structures are being probed (e.g. intrinsic imaging mapping studies (Masino, Kwon et al. 1993; Bonhoeffer, Kim et al. 1995)). In these cases prior information concerning spatial scale and position could be properly exploited to determine the strategy for selecting the parameters on the significance threshold calculations that optimise the power of the test.

4.2 Physiology

There is some interesting, even tantalising physiology in this data. The most striking is the differences between the time series under the red and green illumination conditions. We expected to see differences in the hemodynamics of rCBF in response to stimulation under the different illumination wavelengths because the usual explanation of the intrinsic image data is that there is a rapid early phase of increased post stimulus deoxygenation followed by a later increase in blood volume and flow (Grinvald, Lieke et al. 1986; Frostig, Lieke et al. 1990; Malonek, 1996 #157; Grinvald, Frostig et al. 1991; Mayhew, Askew et al. 1996). However, there is a discrepancy. Malonek (1996) reported finding no decrease in the volume of oxygenated blood though there was an increase in the volume of deoxygenated blood in the period immediately following the stimulation. They suggested that fast capillary recruitment might account for this difference from expectations. Our analysis does not resolve the data into volume proportions of the different forms of hemoglobin as Malonek (1996) did, however we find a clear disassociation with the parameters P1 and P2 under the different illumination conditions which raises a challenge to Malonek's (1996) explanation. Using *'naive oximetry'*, the P1 activity detected under red illumination corresponds to the deoxygenation and the later P2 activity (under green illumination) to an increase in volume. One possibility is that their analysis did not contain sufficient parameters, nor an accurate model of the tissue scattering spectrum. Furthermore there is no mention in their paper of how they compensated for the spectral response of the camera CCD array. They reported using a slow scan CCD camera (which often have compensatory coatings to produce flat spectral sensitivity) and a commercial system. Between the wavelengths 500-700 which they used, the

spectral response of CCD cameras is generally an increasing near linear ramp. This is very similar to estimates of the tissue scattering spectra (MacVicar and Hochman 1991; Kreisman, LaManna et al. 1995). Malonek (1996) used a flat spectrum for this parameter.

The added value of the study we report is that it shows very clearly that the stimulation induced spatial temporal dynamics are different in the various types of vasculature. On the other hand, we found little evidence that the V-signal (~0.1Hz) was systematically different in the different kinds of vessel and parenchyma. However, the V-signal in the first experiment was uncharacteristically weak, particularly under red illumination and we found in the residual maps (Figure 9) a very low frequency component (~0.05 Hz) largely constrained to regions in the veins and capillaries. Data from the second experiment showed large amplitude V-signal oscillation with different spatial distributions and evidence for a difference in phase under the two illumination conditions. The increase in V-signal amplitude induced by reduced MABP differed under the two illumination conditions but these changes were not confined to a particular type of vascularity. After the second withdrawal of blood at a level of MABP where autoregulation begins to fail (Morita, Bouskela et al. 1992), the V-signal under different illumination became desynchronised and the oscillations under green illumination disappeared. This phenomenon has now occurred in three replications of this preparation, and we currently do not have an explanation for it.

Both the above experiments were in cortex. The third, in the periphery (rat testes) showed very clear phase differences between the V-signal under the two conditions of illumination confirming the analysis of Experiment 2. We know of no other study that has reported similar findings. This is further support by the fact that the V-signal obtained under the two illumination conditions can be disassociated. Previously we had thought that the V-signal was the modulation of intensity 'reflecting' the change in absorption produced by changes in the density of hematocrit produced by fluctuations in flow velocity (Fagrell, Fronek et al. 1977; Fagrell, Intaglietta et al. 1980), i.e., modulation of blood volume. This could not produce a phase difference. If the proportions of different hemoglobin derivatives remain constant over the data collection period, then though the absorption (amplitude of the V-signal) will be different under the two illumination conditions the phase and frequency would be similar. Fargrell (1980) found, albeit in the nail fold capillary bed, a phase difference between the modulation of blood flow velocity and the modulation of relative hematocrit density. The changes in flow differed from changes in hematocrit sometimes by as much as 4.5 seconds. Damber(1986) found evidence for similar relationship between flow and hematocrit in the testicular microcirculation of the rat. The hypothesis to explain this is that flow velocity is modulated by changes in the diameter of up stream arterioles and opening of pre-capillary sphincters. The question then becomes how to associate a change in flow with one illumination wavelength and a change in density with another.

4.3 Conjecture

The modulation of flow corresponds to local changes in Nitric Oxide (NO) production and that the changes under the different illumination conditions are due to the interaction of:

1. *spectral changes derived from changes in the volume proportion of oxygenated and deoxygenated hemoglobin and their interaction with NO to form methemoglobin, and nitrosylhemoglobin.*
2. *absorbance changes derived from modulation of the volume of hematocrit.*

Numerous papers attest to the fact that NO is a potent vasodilator, it can act like a transmitter, it is expressed by neurons, glia and endothelium, and is known to be involved both in the

maintenance of resting cerebral blood flow and in the cerebro-vasodilation associated with increased neural activity (Bredt and Snyder 1992; Iadecola 1993; Murphy, Simmons et al. 1993; Garthwaite and Boulton 1995). It is also well known that hemoglobin is a scavenger of NO and that NO interacts with oxyhemoglobin (HbO) to produce methemoglobin (metHb), and with deoxy-hemoglobin (Hb) and methemoglobin to produce nitrosylhemoglobin (HbNO) (Assendelft 1970; Kelm and Schrader 1990; Archer 1993). The spectral changes of oxyhemoglobin to methemoglobin were used by Kelm (1990), albeit in isolated guinea pig hearts, to monitor NO in tissue using difference spectrophotometry, and Jia (1996) proposed a role for S-nitroso-hemoglobin in moderating the scavenging of NO by the heme iron. This study also used spectroscopy to monitor interactions of NO and the different forms of hemoglobin. Jia (1996) proposed a regulatory role for S-nitrosothiols (SNO) which are a form of NO which can be carried by the blood S-nitroso-hemoglobin (SNO-Hb), in contra distinction to NO which is rapidly scavenged by blood. They found that the rate at which SNO-Hb releases SNO groups is influenced by the amount of NO scavenged and also by oxygen tension. They suggested that SNO-Hb provides a mechanism for the delivery and maintenance of the useful biological effects of NO (e.g. regulation of capillary blood flow and mitochondrial respiration) in a form that is safe from inactivation by blood.

Recently Magistretti (1996) suggested that the early decrease in intensity immediately following stimulation detected in intrinsic imagery (Frostig, Lieke et al. 1990; Malonek, 1996 #157) (e.g., the parameter P1 in our analysis) could be due, not as supposed to increased metabolic uptake of oxygen, i.e., the spectral changes of oxygenated to deoxygenated hemoglobin, but to spectral changes produced by the oxidation of oxygenated hemoglobin to met-hemoglobin by NO, or a combination of both.

While this suggestion is extremely interesting and potentially of great importance it is uncertain whether the quantities involved are appropriate, for example, what is the scale of the competition between NO and tissue for the available oxygen carried by blood? We have found in simulation of the intrinsic image signal sources (Mayhew and Zheng 1996) that the intrinsic images were quite sensitive to changes in the parameter for the increase in cerebral metabolic rate for oxygen (CMRO). Although an activity induced increase in deoxygenated hemoglobin closer to 10% rather than the 5% reported by Fox (1986) was needed to produce intrinsic image mapping data similar to that reported in the literature (Frostig, Lieke et al. 1990). This suggests, given the spectral characteristics of HbO and metHb, that the quantities involved may be of similar order, and deoxygenation by both routes is plausible. It is also uncertain whether the methods for estimating CMRO would be sensitive to the deoxygenation produced by the reaction of NO and HbO (the resulting metabolites nitrate and nitrite remain in the blood stream). This is to ask whether the 5% increase in CMRO reported by Fox (1986) results purely from tissue usage distinct from NO scavenging. At the risk of over simplification, the emission scans for measurement of CMRO are derived relatively directly from the quantity of oxygen that has diffused out of the blood stream into the tissue where it is metabolised to water which exchanges back into the intravascular compartment. Corrections for blood flow, arterial saturation and vascular compartment volume are then applied. It is not known whether the labelled products of the NO and Hb interactions affect these measurements. On the other hand, intrinsic imaging mapping studies monitor the spectral changes in the underlying capillaries beds which reflect changes in the different forms of deoxygenated hemoglobin derivatives remaining in the blood supply. The oxygen utilised to maintain neural metabolic activity, and the deoxygenation as the result of the conversion of NO may be largely in different 'compartments' but intrinsic imagery is sensitive to the effective *deoxygenation* by both routes.

In the light of the above, we propose the hypothesis that the V-signal is produced by the interaction of both the modulation of blood volume; i.e., hematocrit density, and the spectral changes produced by the NO interaction with hemoglobin in its different forms. Under green illumination, the interactions are complicated. The peak wavelength of the green illumination (565nm) is approximately at an isobestic point for oxy and deoxygenated hemoglobin (changes from HbO to Hb would have little effect), but changes either to metHb or HbNO could be detected. The change to metHb from HbO would act to decrease absorbance and the change to HbNO from Hb and from metHb acts to increase absorbance above the level for Hb and HbO.

On the other hand, at longer wavelengths (>600nm) the changes from HbO to metHB (and to Hb) act to increase absorbance. The change from metHb to HbNO decreases absorbance back to near the same level as the change from HbO to Hb. Any change from Hb to HbNO would have little effect on absorbance. Under both wavelengths of illumination, increases in volume would be expected to increase absorbance (if the proportions remain constant).

The matter is further complicated by the fact that the proportion of HbNO and metHb formed depends on the oxygenation state of the blood. Using electro paramagnetic spin resonance (EPR) spectroscopy Wennmalm(1992) found (in human) that in arterial blood NO is converted almost completely to metHb with little HbNO, in contrast to venous blood where more HbNO is produced. Furthermore the transition from metHB to HbNO is very slow (Henry, Lepoivre et al. 1993), and to simplify we may ignore the spectral changes from metHb to HbNO.

For arterial blood we would expect the transition from HbO to metHb to produce a decrease in absorbance under green illumination, but under red illumination it would cause an increase in absorbance. Little HbNO would be produced.

For venous (and capillary beds) we would expect both the transitions of HbO to metHB and Hb to HbNO to occur. Under green illumination the first would decrease absorbance and the change to HbNO would increase it (possibly by less) and effects would tend to cancel each other. Under red illumination only the transition from HbO to metHb would affect the absorbance (increasing it).

In the context of neural activity induced changes to rCBF there would be spectral changes produced by deoxygenation, and by increases in volume and flow. These would be coupled with the above spectral effects. The potential interactions in the dynamics of such a system are far too complicated to solve without recourse to a mathematical modelling and our current model of the intrinsic signal (Mayhew and Zheng 1996) is being modified in the light of the above discussion. In the context of the data from the studies of the V-signal, we suggest that it is plausible that the effects of any NO involved interactions are different under the two illumination conditions and that these effects interacting with the spectral results of delayed changes in blood volume could introduce the phase shifts we detect. The test of this hypothesis is a topic awaiting further investigation.

5. References

Andrew, R. D. and B. A. MacVicar (1994). "Imaging cell volume changes and neuronal excitation in the hippocampal slice." Neuroscience **63**(2): 371-383.

Archer, S. (1993). "Measurement of nitric oxide in biological models." FASEB **7**: 349-360.

Assendelft, v. O. W. (1970). Spetrophotometry of Haemoglobin Derivatives, Royal Vangorum Ltd Assen, The Netherlands. Charles C Thomas.

Blasdel, G. G. and G. Salama (1986). "Voltage-sensitive dyes reveal a modular organization in monkey striate cortex." Nature **321**: 579-585.

Bonhoeffer, T., D. Kim, et al. (1995). "Optical imaging of the layout of functional domains in area 17 and across the area 17/18 border in cat visual cortex." Europ. J. Neuroscience: (in press).

Bredt, D. S. and S. H. Snyder (1992). "Nitric oxide, a novel neural messenger." Neuron **8**: 3-11.

Cox, S. B., T. A. Woolsey, et al. (1993). "Localised dynamic changes in cortical blood flow with whisker stimulation corresponds to matched vascular and neuronal architecture of rat barrels." Journal of Cerebral Blood Flow and Metabolism **13**: 899-913.

Damber, J.-E., B. Anders, et al. (1986). "Testicular microcirculation in the rat studied by videophotometric capillaroscopy, fluorescence microscopy and laser Doppler Flowmetry." Acta Physiol. Scand. **126**: 371-376.

Fagrell, B., A. Fronek , et al. (1977). "A microscope-television system for studying flow velocity in human skin capillaries." Am. J. Physiol. **233**(2): H318-H321.

Fagrell, B., M. Intaglietta, et al. (1980). "Relative hematocrit in human skin capillaries and its relation to capillary blood flow velocity." Microvascular Research **20**: 327-335.

Fox, P. T., M. E. Raicle, et al. (1986). "Nonoxidative glucose consumption during focal physiologic neural activity." Science **241**: 462-464.

Friston, K. J., C. D. Frith, et al. (1991). "Comparing functional (PET) images: the assessment of significant change." Journal of Cerebral Blood Flow and Metabolism **11**: 690-699.

Friston, K. J., P. Jezzard, et al. (1994). "Analysis of functional MRI time series." Human Brain Mapping **1**: 153-171.

Friston, K. J., J. Worsley K, et al. (1994). "Assessing the significance of focal activations using their spatial extent." Human Brain Mapping **1**: 214-220.

Frostig, R. D., E. E. Lieke, et al. (1990). "Cortical functional architecture and local coupling between neuronal activity and the microcirculation revealed by in vivo high-resolution optical imaging of intrinsic signals." Proc. Natn. Acad. Sci. U.S.A. **87**: 6082-6086.

Garthwaite, J. and C. L. Boulton (1995). "Nitric oxide signalling in the central nervous system." Annu. Rev. Physiol **57**: 683-706.

Grinvald, A., R. D. Frostig, et al. (1991). "High-resolution optical imaging of functional brain architecture in the awake monkey." Proc. Natl. Acad. Sci. USA **88**: 11559-11563.

Grinvald, A., E. Lieke, et al. (1986). "Functional architecture of cortex revealed by optical imaging of intrinsic signals." Nature **324**: 361-364.

Henry, Y., M. Lepoivre, et al. (1993). "EPR characterisation of molecular targets for NO in mammalian cells and organelles." FASEB J. **7**: 1124-1134.

Iadecola, C. (1993). "Regulation of the cerebral microcirculation during neural activity: is nitric oxide the missing link?" Trends in Neuroscience **16**(6): 206-214.

Jia, L., C. Bonaventura, et al. (1996). "S-nitosohaemoglobin: a dynamic activity of blood involved in vascular control." Nature **380**: 221226.

Kelm, M. and J. Schrader (1990). "Control of coronary vascular tone by nitric oxide." Circ. Res. **66**: 1561-1575.

Kreisman, N. R., J. C. LaManna, et al. (1995). "Light transmittance as an index of cell volume in hippocampal slices: optical differences of interfaced and submerged positions." Brain Research **693**: 179-186.

MacVicar, B. A. and D. Hochman (1991). "Imaging of synaptically evoked intrinsic signals in hippocampal slices." J. Neurosci. **11**: 1458-1469.

Magistretti, P. J. and L. Pellerin (1996). "Cellular bases of brain energy metabolism and there relevance to functional brain imaging : evidence for a prominent role of astrocytes." Cerebral Cortex **6**(Jan/Feb): 50-61.

Malonek, D. and A. Grinvald (1996). "Interactions between electrical activity and cortical microcirculation revealed by imaging spectroscopy: implications for functional brain mapping." Science **272**: 551-554.

Masino, S. A., M. C. Kwon, et al. (1993). "Characterisation of functional organisation within rat barrel cortex using intrinsic signal optical imaging through a thinned skull." Proc. Natl. Acad. Sci. USA **90**: 9998-10002.

Mayhew, J. E. W., S. Askew, et al. (1995). "Cerebral vasomotion: 0.1Hz oscillation in imaging of neural activity." Soc. Neurosci. Abstr. **21**: 656.9.

Mayhew, J. E. W., S. Askew, et al. (1996). "Cerebral vasomotion: 0.1Hz oscillation in reflected light imaging of neural activity." Neuroimage (in press : AIVRU memo 105).

Mayhew, J. E. W. and Y. Zheng (1996). "A model of the intrinsic image signal and an evaluation of the methodology of intrinsic image signal analysis." AIVRU memo 109.

Morita, Y., E. Bouskela, et al. (1992). "Vasomotion in the rat cerebral microcirculation recorded by laser-doppler flowmetry." Acta Physiol. Scand **146**: 431-439.

Murphy, S., M. L. Simmons, et al. (1993). "Synthesis of nitric oxide in CNS glial cells." TINS **16**(8): 323-328.

Thomson, D. (1982). "Spectrum estimation and harmonic analysis." Proc. IEEE **70**(9): 1055-1097.

Thomson, D. (1990). "Quadratic-inverse spectrum estimates: applications to palaeoclimatology." Phil. Trans.R.Soc.Lond. **332**: 539-597.

Thomson, D. (1995). "The seasons, global temperature, and precession." Science **268**: 59-68.

Thomson, D. J. and A. D. Chave (1991). Jacknifed error estimates for spectra, coherences and transfer functions. Ch.2. Advances in spectrum analysis. S. Haykin, Prentice-Hall Englewood Cliffs NJ: 58-117.

Turner, R. and A. Grinvald (1994). "Direct visualisation of patterns of deoxygenation and reoxygenation in monkey cortical vasculature during functional brain activation." Proc. Soc. Magn. Res.: 430.

Wennmalm, A., G. Benthin, et al. (1992). "Dependence of the metabolism of nitric oxide (N)) in healthy humans whole blood on the oxygenation of its red cell haemoglobin." Br. J. Pharmacol. **106**: 19-30.

Woolsey, T. A. and C. M. Rovainen (1991). Whisker barrels: A model for direct observation of changes in the cerebral microcirculation with neuronal activity. Brain Work and Mental Activity: Alfred Benzon Symposium 31, Copenhagen.

Worsley, K. J., A. C. Evans, et al. (1992). "A three dimensional statistical analysis for rCBF activation studies in human brain." J Cereb.Blood Flow Metab. **12**: 900-918.

6. Figures

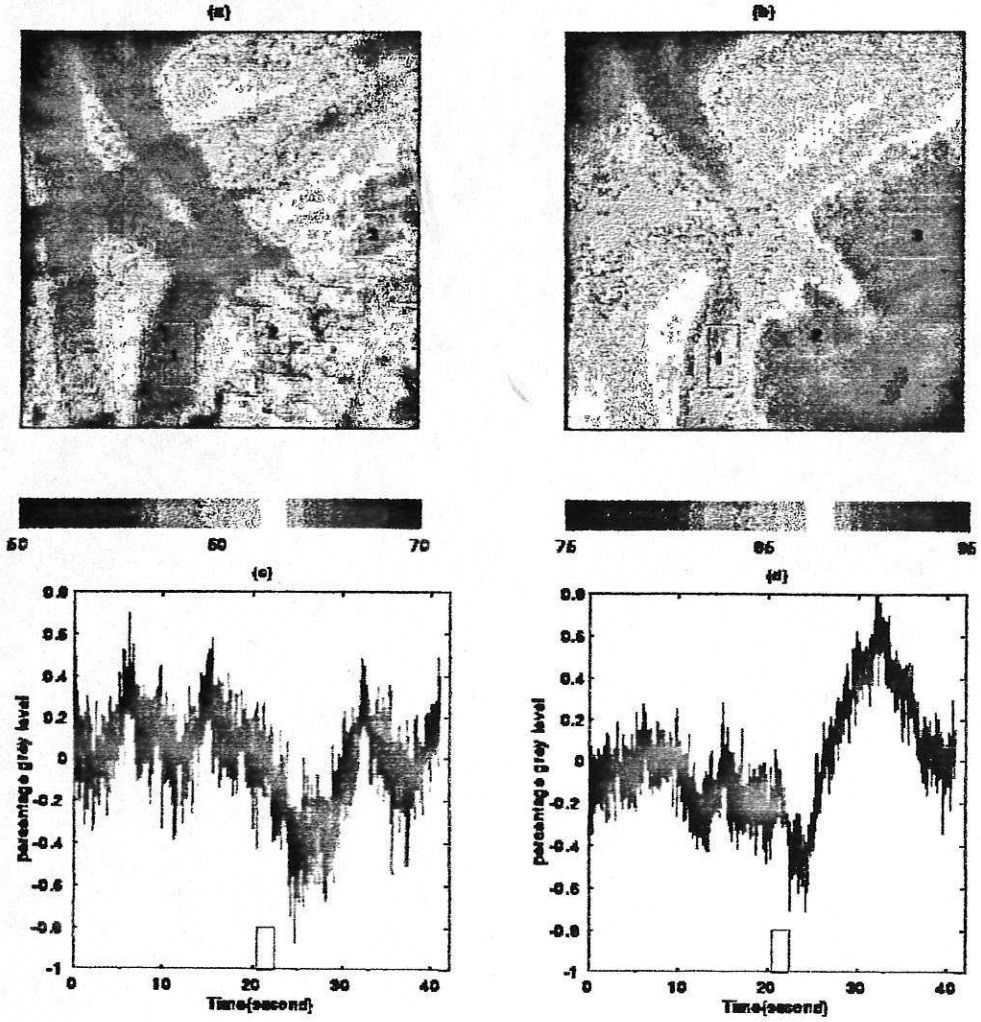

Figure 1. Mean images under (a) green illumination; (b) red illumination. The image subtends a 2×2 mm area (100×100 pixels: 1 pixel = 20 microns). Mean time series under (c) green illumination and (d) red illumination. The bar shows the stimulation duration (2 sec) starting at the 513th frame (20.5 second)

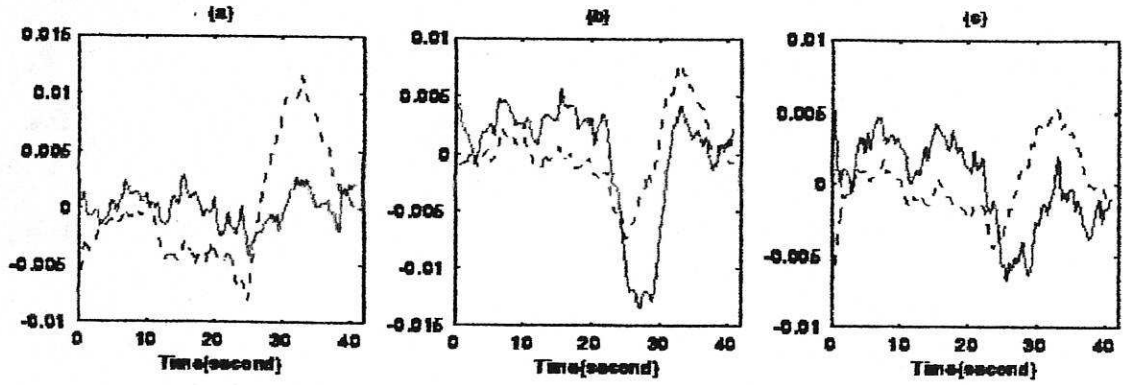

Figure 2. Smoothed mean time series under green illumination (solid line) and under red illumination (dashed line) in (a) venule (area 1), (b) arteriole (area 2) and (c) parenchyma (area 3) .

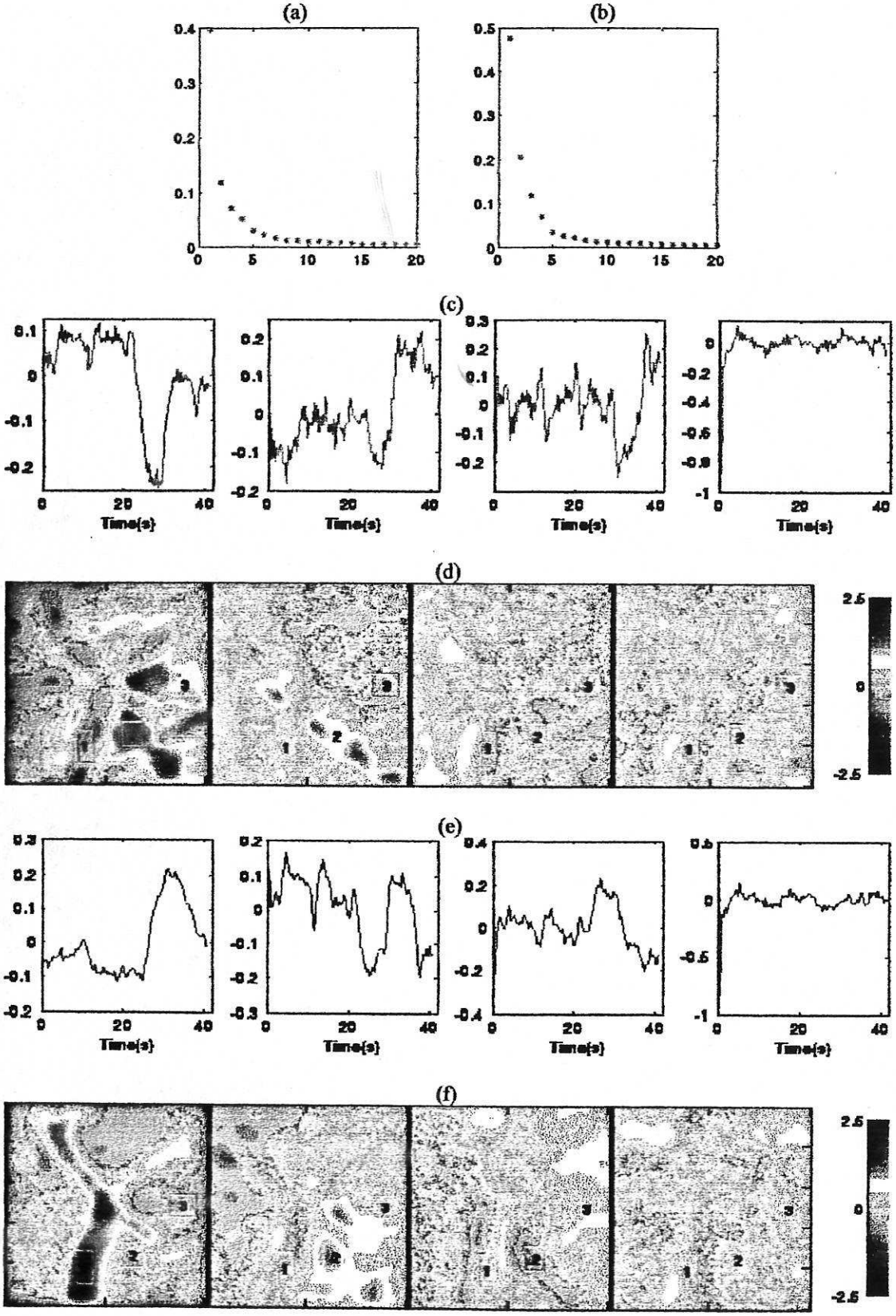

Figure 3. Eigenvalues for (a) green and (b) red illumination. The first four eigenvectors under green illumination are shown in (c) and the first four corresponding eigenimages are shown in (d). The first four eigenvectors under red illumination are shown in (e) and the first four corresponding eigenimages are shown in (f).

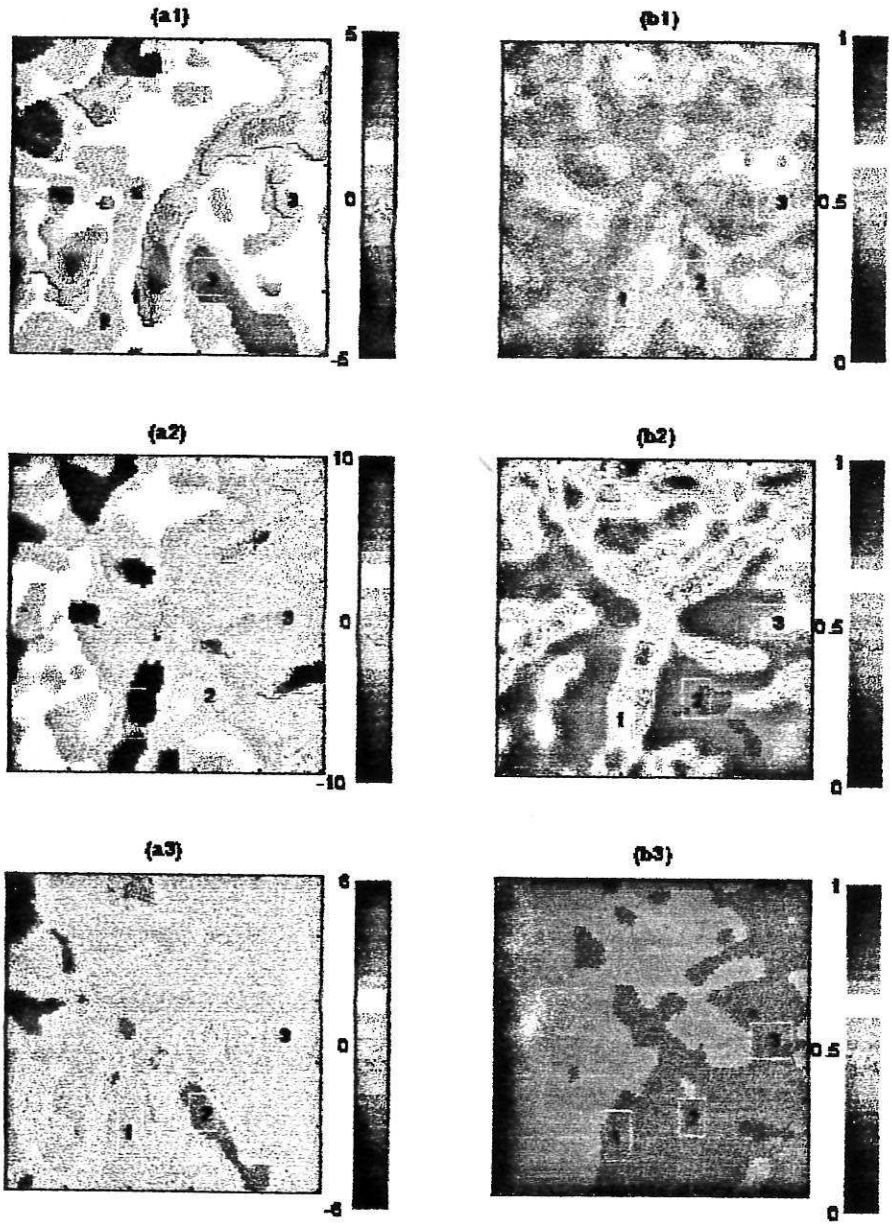

Figure 4. Correlation maps of the '*lags of the maximum correlation*' (right) and the values of the correlation (left) under red illumination (a1, b1 and a3, b3) and under green illumination (a2,b2) with the time series of the haemodynamic models (P1, P2, P3).

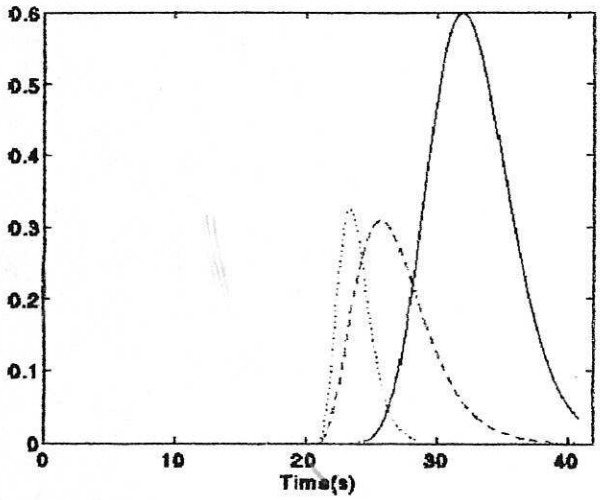

Figure 5. Three gamma functions used in the design matrix to model the undershoot under the red (P1, dotted line) and the green (P2, dashed line) illumination, and the overshoot under the red (P3, solid line) illumination.

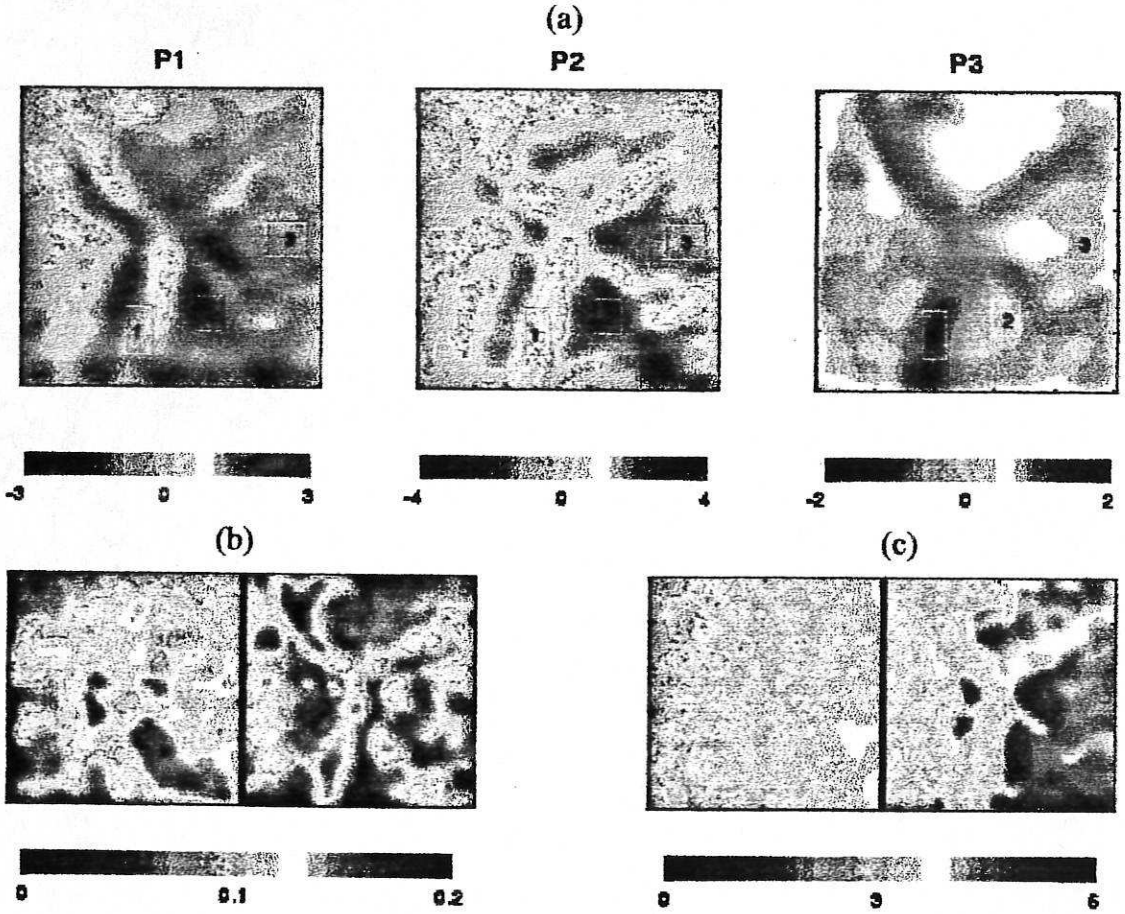

Figure 6. The parameter maps obtained using generalised linear models for (a) the three gamma functions P1, P2 and P3; **(b)** the amplitude (in percentage of grey levels) of the 0.1 Hz oscillation under green (left) and red (right) illumination; and **(c)** the phase (in radians) of the 0.1Hz oscillation under green (left) and red (right) illumination.

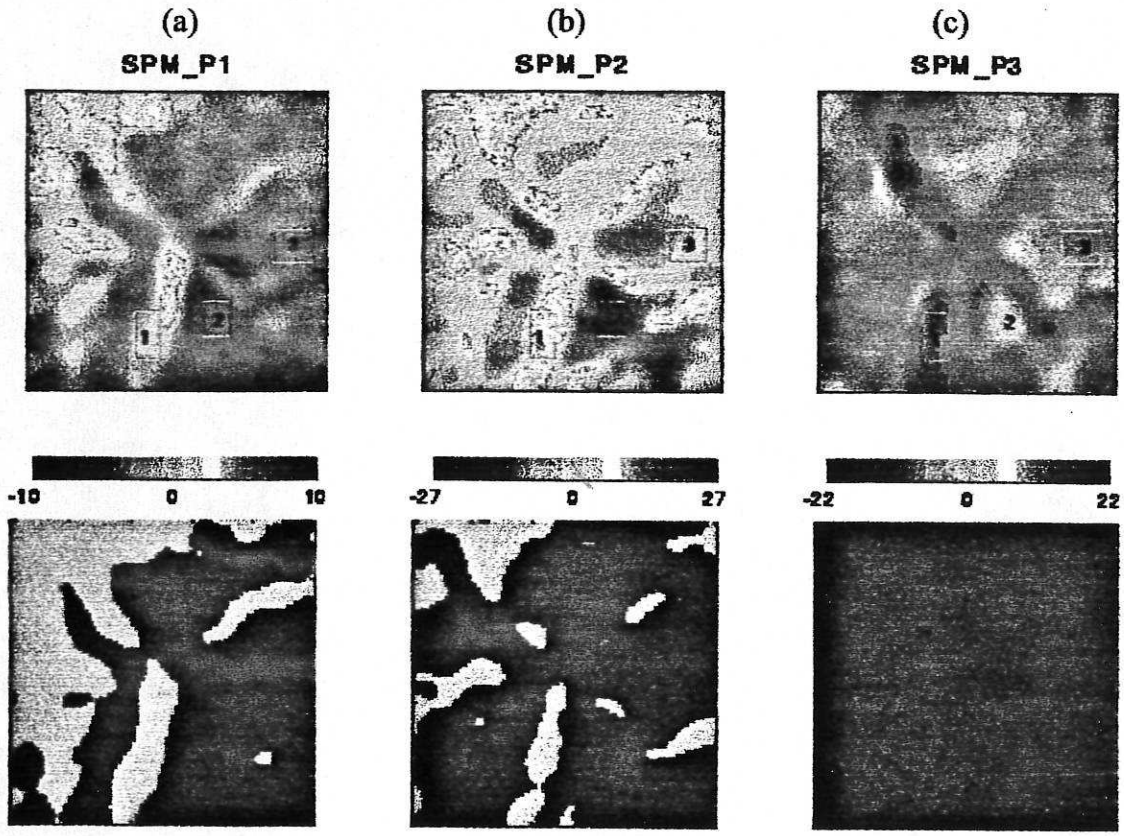

Figure 7. Top row: The SPMs for the neuro-hemodynamic parameters. Bottom row: SPMs thresholded and binarised at the 95% level of confidence (abs(z score) >4.0). The green areas are not significant. **(a)** the undershoot P1 under red illumination; **(b)** the undershoot P2 under green illumination; and **(c)** the overshoot P3 under the red illumination. In **(c)** every pixel reached significance.

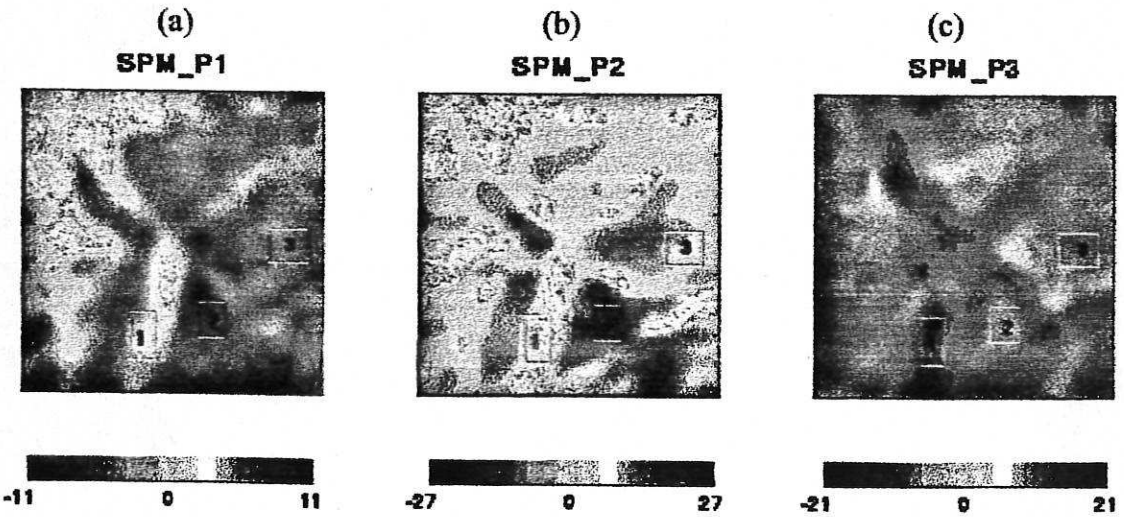

Figure 8. SPMs using the corrected lags in the design matrix for **(a)** the undershoot P1 under red illumination; **(b)** the undershoot P2 under green illumination; and **(c)** the overshoot P3 under the red illumination. The maps are almost the same as those shown in Figure 7.

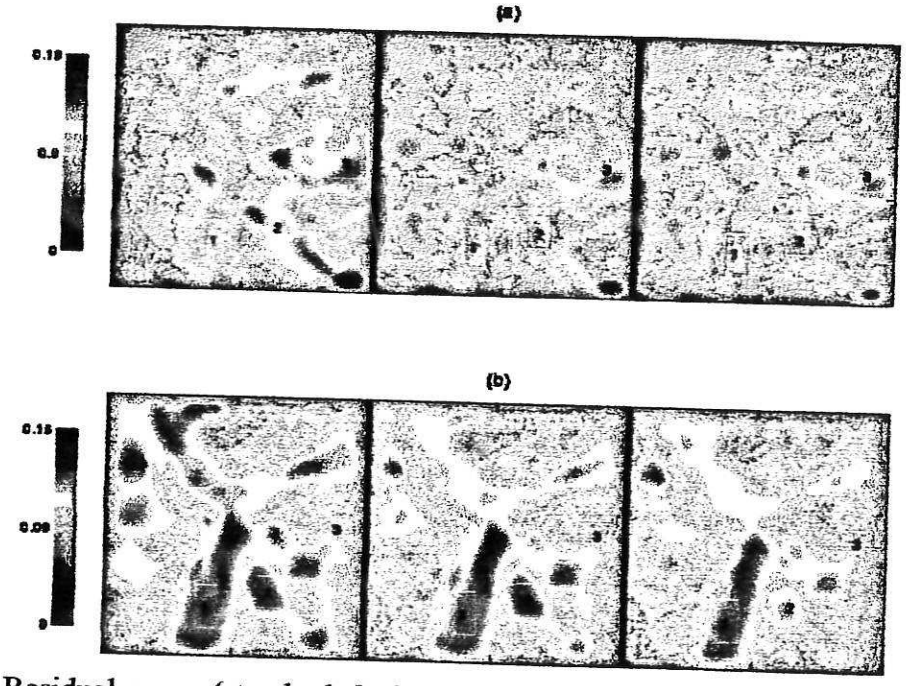

Figure 9. Residual maps (standard deviation of residuals) after analyses using different design matrices (a) under green illumination, (b) under red illumination. (left) including parameters for the V-signal, (middle) excluding parameters for the V-signal, (right) the parameters (P1 P2 P3) corrected with the correlation lags *and* parameters for the V-signal were included in the design matrix.

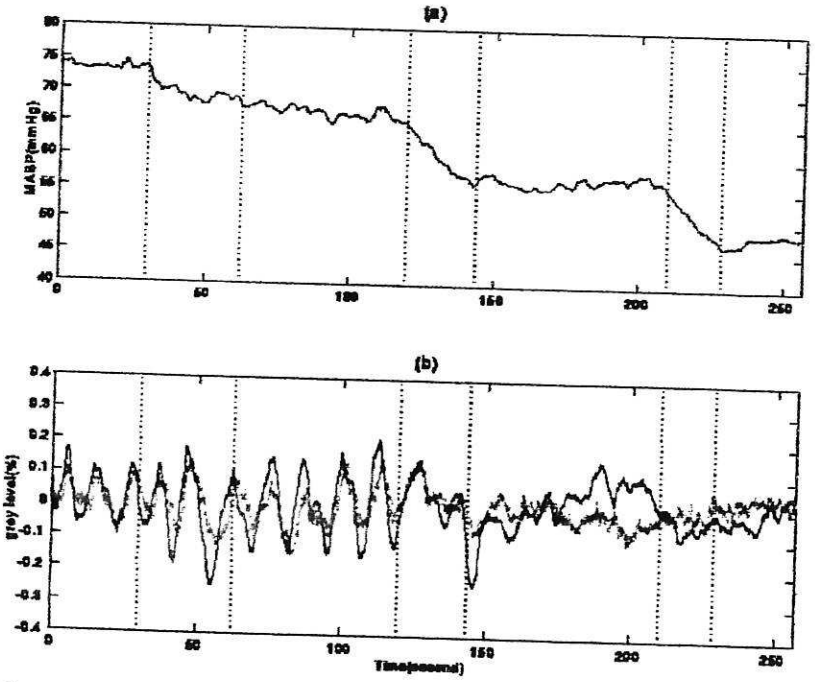

Figure 10 (a) Time series of mean arterial blood pressure (MABP). Dotted markers show periods of blood withdrawal (30-62, 120-144, 210-229). **(b)** Mean time series of image data under red (solid line) and green (dashed line) illumination. Note desynchronisation following the second period of blood withdrawal.

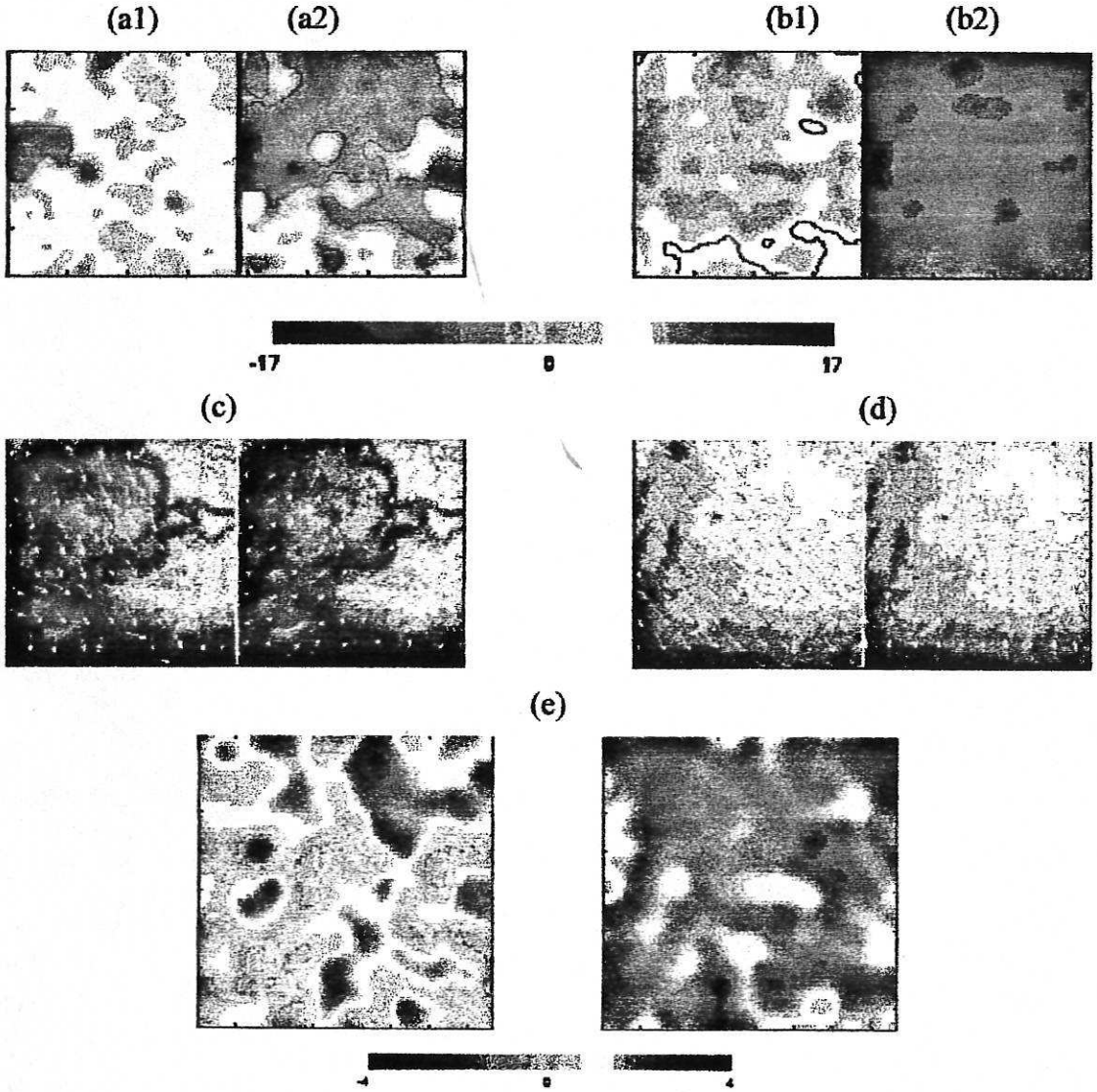

Figure 11 (a) SPMs of the amplitude of the V-signal before **(a1)** and after **(a2)** blood withdrawal under green illumination. **(b)** SPMs of the amplitude of the V-signal before **(b1)** and after **(b2)** blood withdrawal under red illumination. **(c and d)** Corresponding angle maps showing phase of the V-signal. The arrows indicate the phase with respect to the horizontal axis. **(e)** SPMs of the *before and after* differences in amplitude of the V-signal for the green (left) and red (right) illumination conditions. The 'z' scores for the 95% confidence level is 4.75. in maps **(a)** and **(b)** and contours have been superimposed to show the significant areas. The 95% confidence level for the difference test is 4.0 in (e) Almost no pixels achieved significance so the contouring was ommitted.

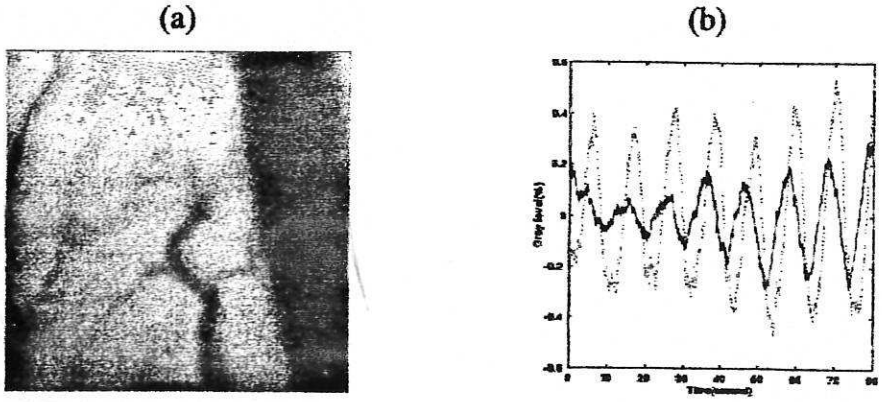

Figure 12. (a) Image of surface microvasculature of rat testes under green illumination. **(b)** Mean time series under green (dotted line) and red (solid line) illumination. The apparent single large vessel on the right is actually an overlapping artery and vein.

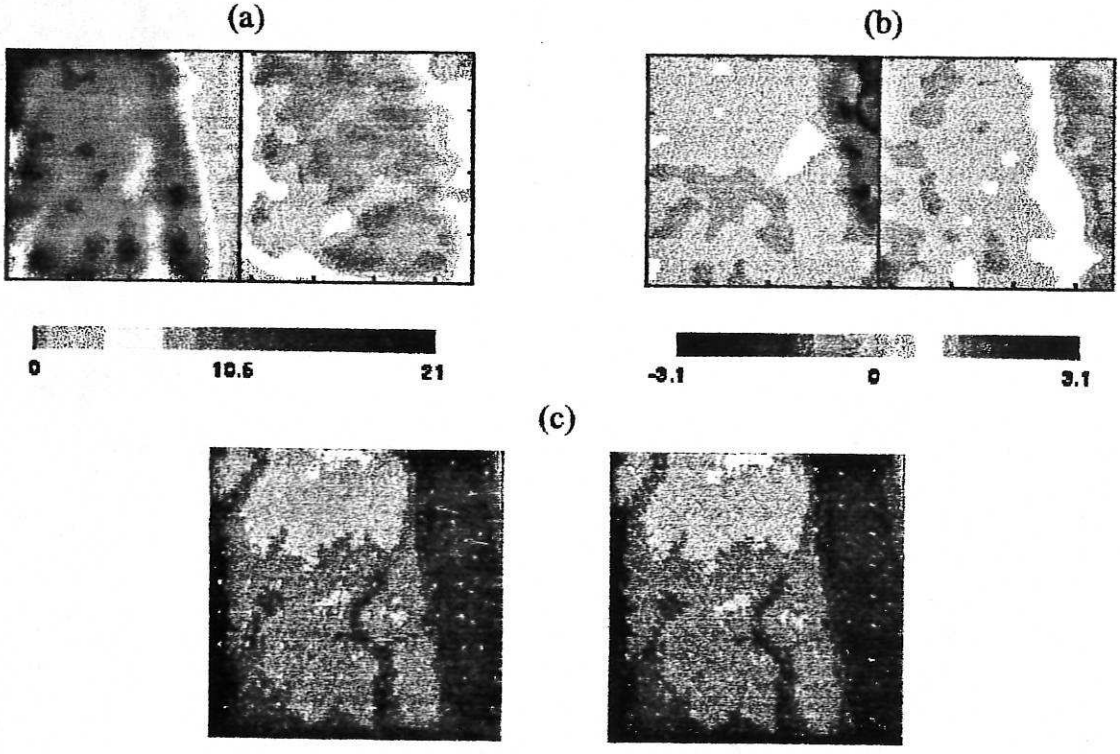

Figure 13 (a) SPMs of amplitude of the V-signal under green (left) and red (right) illumination. The colour scale shows the 'z' score (95% confidence level 4.75). (b) maps of the phase of the V-signal under green (left) and red (right) illumination. The scale shows the phase angle in radians. The phase under green illumination has been shifted by 1.1 radians relative to that under red illumination to facilitate comparison. (c) Angle maps of phase superimposed on the images of the vascularity. The arrows indicate the phase of V-signal with respect to the horizontal axis. Under green illumination, the estimates of phase in the region corresponding to the vessels on the right should be regarded as unreliable as V-signal amplitude in this region is not significant.

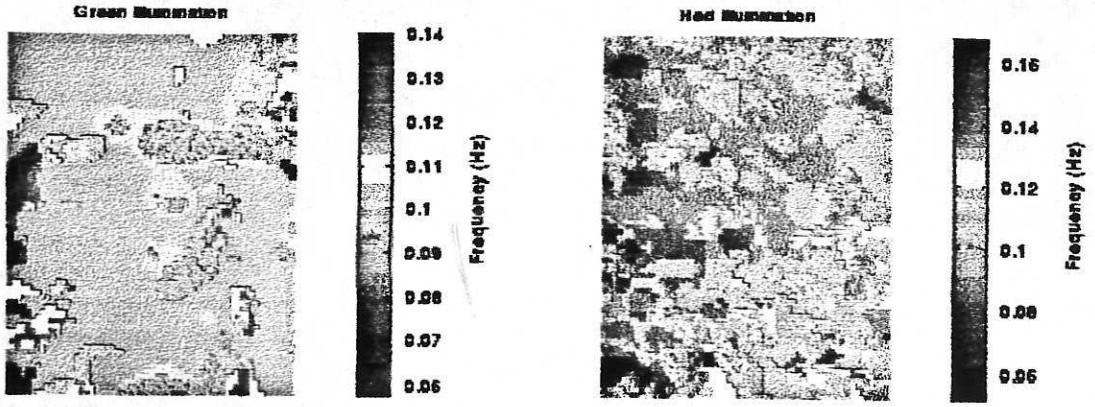

Figure 14. Maps of the frequencies under green (left) and red (right) illumination using iterated complex demodulation. The slight right bottom to left top trend in frequency under red illumination may be responsible for the trend in the same direction that can be seen in the phase maps of Figure 13(b).

Appendix I: Statistical Parametric Maps (SPMs)

Statistical parametric maps (SPMs) are images whose pixel values are distributed, under the null hypothesis, according to some known probability density function.

Consider the linear model :

$$X = G\beta + e \tag{1}$$

where X is the temporal data vector of a pixel after removal of mean under null stimulus, G is the design matrix, β is the parameter vector corresponding to each component of G, and e is the noise vector of normally distributed with mean zero and covariance matrix $\sigma^2 \cdot I$.

X is smoothed by multiplying by a matrix K, then the design matrix becomes $G^* = KG$.

The least square estimate of the parameter vector in this case is:

$$\hat{\beta} = (G^{*T} G^*)^{-1} G^{*T} KX \tag{2}$$

If the design matrix G is independent of the noise e, then the above estimate is unbiased. The covariance matrix of $\hat{\beta}$ is

$$\mathrm{cov}(\hat{\beta}) = \sigma^2 (G^{*T} G^*)^{-1} G^{*T} KK^T G^* (G^{*T} G^*)^{-1} \tag{3}$$

The unbiased estimate of the variance of the noise is given by

$$\hat{\sigma}^2 = (RKX)^T (RKX) / \mathrm{trace}(RKK^T) \tag{4}$$

where R is the residual-forming matrix given by

$$R = I - G^* (G^{*T} G^*)^{-1} G^{*T} \tag{5}$$

Statistic Test

Null Hypothesis: The action of an interested biological effect (including intrinsic signals and stimuli) is absent in the brain activity, i.e., the contribution of a selected ith column in the design matrix to the observation data vector X is zero. This is equivalent to saying that the ith element β_i in $\hat{\beta}$ corresponding to the interested biological effect is zero.

In order to select the ith element from a vector, a contrast vector c is introduced such that the ith element in c is unity while all the other elements are zero.

Now let

$$Z = c\hat{\beta} / [c\hat{\sigma}^2 (G^{*T} G^*)^{-1} G^{*T} KK^T G^* (G^{*T} G^*)^{-1} c^T]^{1/2} \tag{6}$$

It can be shown that Z satisfies a t-distribution with degrees of freedom ν given by:

$$\nu = \mathrm{trace}(RKK^T)^2 / \mathrm{trace}(RKK^T RKK^T) \tag{7}$$

When the degrees of freedom is large enough, typically when $\nu > 45$, the above t- distribution is approximated by a normal distribution. A pixel is said to be significantly activated by the ith effect if its Z score is bigger than certain level of significance.

The above significance test is applicable to individual pixels assuming they are independent of each other. In reality, images are often spatially smoothed to reduce noise and enhance spatial coherence. Friston and Worsley *et al.* have studied the probability of finding the significant areas in the Gaussian random fields. Their results are summarised as follows.

(1) The probability of getting at least one pixel with a Z score greater than u, in a D dimensional SPM$\{Z\}$ of volume V is the same as the probability of having the largest Z score in the entire volume (Z_{max}) greater than u, i.e.,

$$P(Z_{max} > u) \leq E\{m\} \approx V \cdot (2\pi)^{-(D+1)/2} W^{-D} u^{D-1} \exp(-u^2/2) \tag{8}$$

where $E\{m\}$ is the expected number of maxima. W is a measure of spatial smoothness and is related to the full width at half maximum (FWHM) of the SPM (Friston *et al.*, 1995).

In practice W can be determined directly when Gaussian blur is used to process the image sequence in spatial domain, $W = \sqrt{2}\sigma_0$, where σ_0 is the standard deviation of Gaussian smoothing function.

In the situation of two dimensional image, i.e., D=2, the volume V is the area of the image, denoted as S, and Eq. (7) becomes:

$$P(Z_{max} > u) \leq E\{m\} \approx S \cdot (2\pi)^{-3/2} 2^{-1} \sigma_0^{-2} u \exp(-u^2/2) \cdot \tag{9}$$

the approximation holds if u is sufficiently high.

In our image analysis, *S=100*100*. If $\sigma_0 = 3$ in Gaussian smoothing, then the 5% level of significance for u is obtained by equating

$$P(Z_{max} > u) = 0.05 \tag{10}$$

yielding,

$$u \approx 3.985$$

(2) The probability of getting one or more regions of size k or more in a given SPM$\{Z\}$ of volume V, thresholded at u, is the same as the probability that the largest region (n_{max}) consists of k or more pixels where

$$P(n_{max} \geq k) = 1 - \exp[-E\{m\} \cdot \exp(-\rho k^{2/D})] \tag{11}$$

and

$$\rho = [\Gamma(D/2+1) \cdot E\{m\} / V \cdot \phi(-u)]^{2/D} \tag{12}$$

where $\phi(-u)$ is the integral of the unit Gaussian distribution evaluated at the threshold chosen ($-u$), $\Gamma(\cdot)$ is the gamma function (Friston *et al.*, 1995).

In the situation of two dimensional images, i.e., D=2, , the volume V is the area of the image S . If $P(n_{max} \geq k_\alpha) = \alpha$, where α is suitable small, say 0.05, then we have:

$$k_\alpha = (1/\rho) \cdot \log[-E\{m\} / \log(1-\alpha)] \tag{13}$$

For instance, if *S=100*100* and the point spread function is Gaussian with standard deviation $\sigma_0 = 3$, and if the threshold is taken as u=3, then:

$$P(n_{max} \geq 20) \approx 0.05 \tag{14}$$

However if the activation areas are highly inter-connected, Eq. (11) is difficult to use.

(3) Let $X_1(t),\cdots,X_n(t), t \in R^D$, be independent, identically distributed, homogeneous, real-valued Gaussian random fields each with zero mean and unit variance. Then Adler (1981, p169) defines the χ^2 field $U(t)$ as

$$U(t) = \sum_{i=1}^{n} X_i^2(t), t \in R^D. \tag{15}$$

The distribution of $U(t)$ at each t is χ^2 with n degrees of freedom.

Let $U_{\max} = \sup\{U(t): t \in C\}$ where C is a fixed set. Then

$$P(U_{\max} \geq u) \rightarrow \frac{\lambda(C)\det(\Lambda)^{1/2} u^{(n-D)/2} \exp(-u/2)}{(2\pi)^{D/2} 2^{(n-2)/2} \Gamma(n/2)} u^{D-1} \quad \text{as } u \rightarrow \infty, \tag{16}$$

where $\lambda(C)$ is the Lebesgue measure of C, Λ is the covariance matrix of the blur function (Worsley, 1994).

Let $X_1(t), X_2(t), t \in R^2$ be the statistical parametric maps (SPMs) of the amplitudes of sine and cosine components of vasomotor oscillation signals. Then with n=D=2, we have

$$U(t) = X_1^2(t) + X_2^2(t), \qquad t \in R^2 \tag{17}$$

and

$$P(U_{\max} \geq u) = \frac{S \exp(-u/2)}{2\pi\sigma_0^2} u \quad \text{as } u \rightarrow \infty, \tag{18}$$

where S is the area of the image, σ_0 is the standard variance of Gaussian blur function. If S=100*100, $\sigma_0 = 3$, then the 5% level of significance for u is obtained by letting

$$P(U_{\max} \geq u) = 0.05 \tag{19}$$

yielding,

$$u \approx 22.55$$

The general procedure for obtaining SPM in our image analysis is summarised as follows.

1. Remove mean from each pixel. Then smooth and subsample each pixel in time.
2. Smooth each image using a Gaussian mask. Then subsample each image in space if necessary.
3. Form the design matrix G which includes all the effects of interest (e.g., sine, cosine, gamma functions etc.). Each effect forms a column in G.
4. Estimate $\hat{\beta}$ and $\hat{\sigma}^2$ using Eq.s (2) and (4) respectively.
5. For a particular effect of interest, obtain SPM(Z) and SPM(χ^2) from Eq.s (6) and (17) respectively.
6. Find thresholds for SPM(Z) and SPM(χ^2) using Eq.s (9) and (18) respectively, hence obtain the significance map of the particular effect of interest over the whole image.

Appendix II: Principal Component Analysis (PCA)

Let $A(m,n,N)$ represent a stack of N images of size $(m \times n)$. Thus there are $(m \times n)$ pixels each of which is a time series of length N. Let $p(i,j)$ represent the grey level of the pixel (i,j), $i = 1,\cdots,m$, $j = 1,\cdots,n$. The principal component analysis (PCA) can be carried out by treating each image as a *variable* and each pixel as an *observation* as follows.

1. Remove the mean from each image $A(m,n,k)$, $k = 1,\cdots,N$. Denote $x(k) = A(m,n,k)$ so that $x(1), x(2),\cdots, x(N)$ represent N variables.

2. Form the $(N \times N)$ covariance matrix of the variables as

$$C = \begin{bmatrix} \text{cov}[x(1),x(1)] & \text{cov}[x(1),x(2)] & \cdots & \text{cov}[x(1),x(N)] \\ \text{cov}[x(2),x(1)] & \text{cov}[x(2),x(2)] & \cdots & \text{cov}[x(2),x(N)] \\ \cdot & \cdot & \cdot & \cdot \\ \text{cov}[x(N),x(1)] & \text{cov}[x(N),x(2)] & \cdots & \text{cov}[x(N),x(N)] \end{bmatrix} \qquad (1)$$

3. Find the eigenvectors $v_1,\cdots,v_N$ and the corresponding eigenvalues $\lambda_1,\cdots,\lambda_N$ of the above covariance matrix such that $\lambda_1 >,\cdots,> \lambda_N$.

4. The first eigenvector gives the principal time course of the image stack.

5. Back-projecting all pixels onto the lth eigenvector yields the lth principal eigenimage, given by

$$B_l(i,j) = \sum_{k=1}^{N} p(i,j,k)v_l(k), \qquad i = 1,\cdots,m; \qquad j = 1,\cdots,n. \qquad (2)$$

Appendix III: Complex Demodulation (CDM)

If a time series contains significant energy within a specific frequency band a suitable analysis technique is complex demodulation.

For a time series $x(t)$ complex demodulation estimates the amplitude and phase by forming the complex demodulate

$$y(t) = h(t) * \left\{ x(t) \cdot e^{-i2\pi ft} \right\} = \sum_{j=0}^{N-1} h(j) \cdot x(t-j) \cdot e^{-i2\pi ft} \tag{1}$$

where the phasor $e^{-i2\pi ft}$ shifts the components of $x(t)$ at frequency f to the origin of the complex plane. The operator $*$ represents convolution, and $h(t)$ is the impulse response of a selected low pass filter.

From the complex demodulate the amplitude is estimated by

$$A(t) \approx 2|y(t)| \tag{2}$$

and the phase is estimated by

$$\theta(t) \approx \arctan \frac{\mathrm{Im}\{y(t)\}}{\mathrm{Re}\{y(t)\}} \tag{3}$$

If the assumed centre frequency f is incorrect, the phase $\theta(t)$ will show a linear trend in time. The gradient of this trend is equal to the difference between f and the true frequency. Regression on phase is a standard method for making accurate unbiased frequency estimates.

The process is iterated with improved estimates of the frequency f until the phase $\theta(t)$ has no linear trend. The estimated phase of the signal is the mean of $\theta(t)$.